



## Original Article

## Neutron diagnostics using nickel foil activation analysis in the KSTAR

San Chae<sup>a, b, \*</sup>, Jae-Yong Lee<sup>b</sup>, Yong-Soo Kim<sup>b</sup><sup>a</sup> Korea Atomic Energy Research Institute, 989-111 Daedeok-Daero, Yuseong, Daejeon, Republic of Korea<sup>b</sup> Hanyang University, 222 Wangsimni-ro, Seongdong-gu, Seoul, 133-791, Republic of Korea

## ARTICLE INFO

## Article history:

Received 23 September 2020

Received in revised form

22 February 2021

Accepted 22 March 2021

Available online 30 March 2021

## Keywords:

Neutron activation analysis

KSTAR

Neutron yield

Gamma spectroscopy

MCNP

## ABSTRACT

The spatial distribution and the energy spectrum of the neutron yield were investigated with the neutron activation analysis and MCNP simulation was carried out to verify the analysis results and to extend the results to a 3D mapping of the neutron yield distribution in the KSTAR. High purity Ni specimen was selected in the neutron activation analysis. Total neutron yields turned out to be  $3.76 \times 10^{12}$  n/s –  $7.56 \times 10^{12}$  n/s at the outer vessel of the KSTAR, two orders of magnitude lower than those at the inner vessel of the KSTAR, which demonstrates the attenuation of neutron yield while passing through the different structural materials of the reactor. Based on the fully expanded 3D simulation results, 2D cross-sectional distributions of the neutron yield on XY and ZX planes of KSTAR were examined. The results reveal that the neutron yield has its maximum concentration near the center of blanket and decreases with increasing proximity to the vacuum vessel wall.

© 2021 Korean Nuclear Society, Published by Elsevier Korea LLC. This is an open access article under the CC BY-NC-ND license (<http://creativecommons.org/licenses/by-nc-nd/4.0/>).

## 1. Introduction

Thermonuclear fusion reactors have been highly demanded in the present world undergoing climate change owing to their potential to supply clean energy. Thus research and development for fusion reactors have been carried out worldwide and documented. Great example is the ITER (International Thermonuclear Experimental Reactor) project, which is a mega-experimental engineering project to develop tokamak fusion reactor in Korea, we have studied certain aspects of magnetic fusion energy technology development pertinent to the ITER fusion project as a part of the international contribution through KSTAR (Korea Superconducting Tokamak Advanced Research). KSTAR is a magnetic fusion device that was constructed and has been operating in Korea since June 2008.

KSTAR uses the D-D reaction, so it generates 2.45 MeV neutron in the plasma from the fusion reaction. In the case of D-D fusion reactors, upgraded heating system is required to ignite the fusion reaction because it needs higher energy than D-T reaction. Thus, KSTAR employs various heating technologies: neutral beam injection (NBI), electron cyclotron heating (ECH), and ion cyclotron range of frequency heating (ICRH) [1,2].

Increasing the plasma source power accompanies serious interactions between the tokamak structures and plasma beam ions

avoidably leading to nuclear heating, radiation damage, and activation of shielding and material activation of the structure [3–9]. Therefore, to understand and evaluate the impact of the phenomena, we need to know the neutron flux and its energy distribution in the tokamak system, critically including the components between inboard and outboard vacuum vessel walls.

Fundamentally, there are two approaches to measure of neutron flux spectra for fusion reactor and other nuclear facilities: direct diagnostic system using neutron detectors (fission chambers, proportional counters, scintillators, etc.) and indirect measurements using neutron activation analysis [4,10]. The neutron diagnostic system using fission chamber and bubble detector has been already installed in the KSTAR to measure the neutron flux to the wall [5]. But it can give us only local information on the flux with average kinetic energy, leading to the limited understanding of the phenomena.

On the contrary, if well-designed with appropriate target foils, the activation analysis can be used to obtain the information on both local and total neutron yield with its energy spectrum over the whole fusion reactor system [11,12]. The activation specimens are generally installed at the inboard wall of the reactor to evaluate the neutron yield of the fusion reaction and the analysis measurements of the activated target specimen are carried out with gamma

\*Corresponding author. Hanyang University, 222 Wangsimni-ro, Seongdong-gu, Seoul, 133-791, Republic of Korea.

E-mail address: [lucifer06@hanyang.ac.kr](mailto:lucifer06@hanyang.ac.kr) (S. Chae).

spectroscopy equipped with pneumatic transfer system and vacuum counting system [13,14].

Despite the ultimate need, however, the neutron flux distribution with its energy spectrum in the KSTAR has not been thoroughly evaluated until now. In this study, therefore, the neutron activation analysis was designed to obtain the information on not only the neutron yield but also the neutron energy spectrum throughout whole KSTAR system. Appropriate target foil was selected, and prepared specimens were deployed especially in the proper places of the KSTAR. Then, the Monte Carlo code simulation was followed to verify the analysis results and extend the results to 3-D mapping of the neutron yield and neutron energy distribution in the KSTAR system. For the Monte Carlo simulation, MCNP (Monte Carlo N-Particles Transport) code [15] was used. Usually activation analysis using MCNP are commonly used for the fusion reactor application [16].

## 2. Experimental works

### 2.1. Preparation of activation analysis

As mentioned, KSTAR produces 2.45 MeV neutrons through the D-D fusion reaction. For successful activation analysis, thus, nuclear reaction energy between the target nuclide and the fast neutron is supposed to be lower than this energy and half-life of the reaction product decay should be short but not less than a few days. This limits the selection of right target nuclide for the analysis. Fortunately,  $^{58}\text{Ni}(n, p)^{58}\text{Co}$  reaction was found to be suitable in these conditions, though the nuclide mainly undergoes following two reactions with the fast neutrons:  $^{58}\text{Ni}(n, p)^{58}\text{Co}$  and  $^{58}\text{Ni}(n, \gamma)^{59}\text{Ni}$ . For reference,  $^{58}\text{Co}$  principally decays by emitting 810.8 keV gamma ray with the half-life of 70.8 days [4]. Nickel-58 is the most abundant isotope of nickel, making up 68.077% of the natural abundance, and  $^{58}\text{Co}$  (daughter isotope) emit gamma ray with 98.45%. Therefore, 810.8 keV gamma ray is measured with high probability.

Therefore, high purity Ni specimen (purity: 99.99%) was prepared in a cylindrical disk with dimensions of 3 mm diameter and 3 mm thickness. The nuclear reaction data necessary for this analysis are given in Table 1. Then, totally of 12 Ni specimens were installed at various locations that are indispensable for the evaluation of the neutron yield distribution in the KSTAR system. Fig. 1 shows the locations at outer vessel: J port, F port, P port, and M port, and 3 specimens were installed at each port. The specimens were encapsulated in a high-density polyethylene cylindrical capsule with a diameter of 27 mm and a height of 30 mm. After irradiation, a pneumatic transport system needs not due to low radiation enough from the specimens.

### 2.2. Activation measurement and counting system

Measurement and counting system of the neutron activation analysis consists of high purity germanium (HPGe) detector, a multi-channel analyzer, and a high voltage power supply. To measure the gamma spectrum, a HPGe Coaxial detector (GEM30P4-105 83, AMETEK ORTEC, USA) was used. To achieve low spectroscopic background, the detector and the activated foil sample were

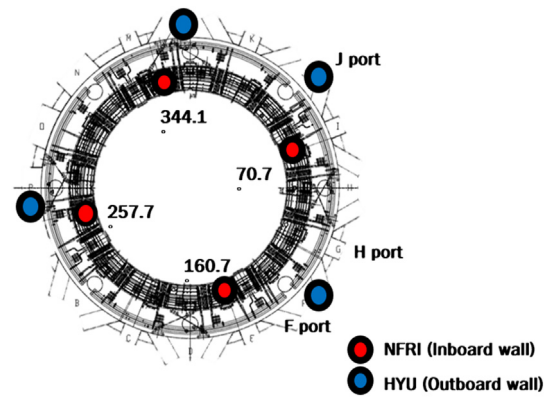


Fig. 1. Installing location of Ni specimens at KSTAR.

placed in a pure lead cylindrical housing.

Detector system was cooled by liquid nitrogen to reduce thermal and electric noise caused by thermal effects in the semiconductor. The energy resolution of the counting system is 1.85 keV full width at half maximum (FWHM) at 1.33 MeV by  $^{60}\text{Co}$ . To identify of the peak, energy calibration was performed using standard gamma sources, i.e.,  $^{137}\text{Cs}$  (661.63 keV) and  $^{60}\text{Co}$  (1173.2 and 1332.5 keV).

For evaluation of precise counts, a counting system need efficiency calibration. There are two methods for efficiency calibration (1) the experimental method (2) the Monte Carlo method. In this study, we performed both the experimental method and the Monte Carlo using MCNP (Monte Carlo N-Particles Transport) code.

To obtain the efficiency at a specific energy, an effective method to help in calibrating and in computing correction factors to be the Monte Carlo simulation. The counting system is constructed in 3D model and shown in Fig. 2. The simulation model consists of detector housing, electrode, detector crystal and lead shield. And a point source, which has 811 keV energy in order to simulate energy with  $^{58}\text{Co}$ , is located on the detector housing.

Also, efficiency calibration was also performed using experimental method. A sealed radioactive source of  $^{54}\text{Mn}$  ( $\gamma$  energy: 834.8 keV) was placed on the detector housing and total the peak intensities within the 834.8 keV energy peak. Compared to other sealed radioactive source,  $^{58}\text{Co}$  is not used well as a seal source due to very short half-life (70.8 days). Therefore,  $^{54}\text{Mn}$  standard seal source which has similar energy with  $^{58}\text{Co}$  and appropriate half-life was used for efficiency calibration at about 800 keV. The efficiency calibration was calculated based on Eq. (1).

$$\epsilon_F = \frac{N_p(E)}{A \cdot I_\gamma(E)} \quad (1)$$

Where A is the total of peak intensities within the energy (Bq),  $I_\gamma(E)$  is emission probability of the gamma ray (99.976%, 834 keV gamma ray), and  $N_p(E)$  is the peak net area. As shown in Fig. 3, the results of experimental method and the Monte Carlo method are 4.4%, 4.8%. Because efficiency results show a similar value between two methods, Monte Carlo method will be used to analysis data evaluation.

Table 1  
Neutron activation reaction used in this work.

Reaction	Reaction Threshold (MeV)	$\sigma$ (barns)	Half life	$\gamma$ Energy (MeV)	$\gamma$ Emission probability per decay (%)
$^{58}\text{Ni}(n, p)^{58}\text{Co}$	0	0.106	70.8 d	0.8108	99.45
$^{58}\text{Ni}(n, \gamma)^{59}\text{Ni}$	0	0.106	$7.6 \times 10^4$ y	1.072	77.9

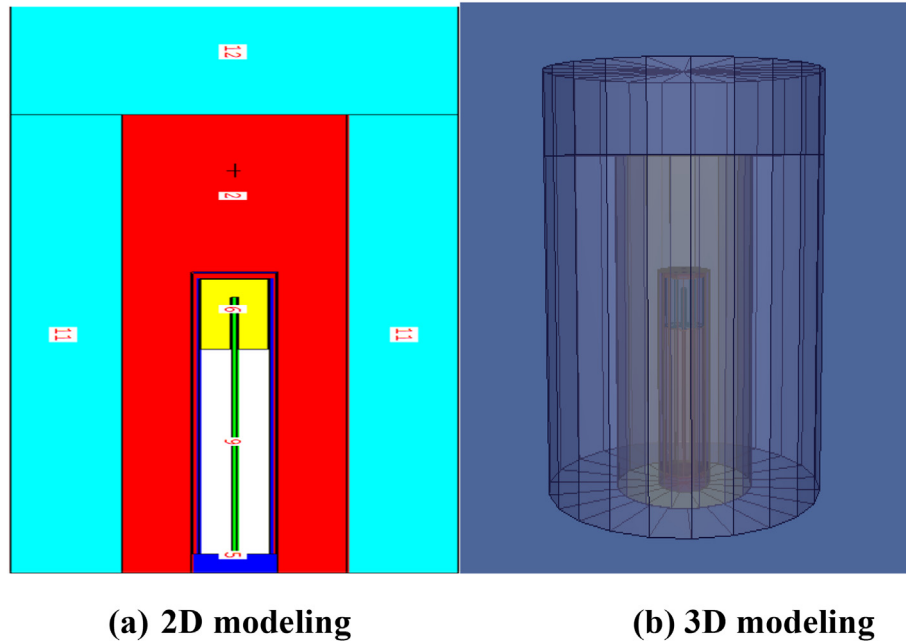


Fig. 2. MCNP simulation model of HPGe detector for efficiency calibration.

### 3. Results and discussion

#### 3.1. Neutron yield determination by neutron activation analysis

KSTAR operated for 10 days with an average of 10 shots in a day while the activation specimens were loaded. Therefore, Ni specimens were irradiated for a total of 20 min. Then, after a cooling period, gamma rays emitted from the  $^{58}\text{Ni}$  were measured with HPGe system. Taking into account the efficiency of the HPGe detector, the activity was calculated from the gamma peak area according to Eqs. (2) and (3) [17].

$$A_{lab} = N\sigma_{eff}\phi\Gamma_{rad}(1 - e^{-\lambda t_a})e^{-\lambda t_w}\left(\frac{1 - e^{-\lambda t_c}}{\lambda t_c}\right) \quad (2)$$

$$A = A_{lab}/\epsilon_F \quad (3)$$

where  $N$  is the number of target atoms,  $\sigma_{eff}$  is the cross-section of  $^{58}\text{Ni}(n, p)^{58}\text{Co}$  reaction,  $t_a$  is the activation time,  $t_w$  is the time between the end of activation and the start of the counting,  $t_c$  is counting time (40000s),  $\lambda$  is the decay constant and  $\Gamma_{rad}$  is the gamma-ray emission probability, i.e. radiation proportion of emitted gamma rays. Efficiency factor so-called ‘efficiency of full absorption peak’, resulting from experimental error such as detector efficiency and detector self-absorption due to the detector geometry, was corrected. We used an average value, 0.106 barn, for effective (n,p) cross-section of neutron from ENDF/B-VII.1 database [18] which was calculated and weighted under 2.45 MeV.

Then, the neutron flux exposed to each specimen was calculated based on following equation:

$$\phi = \frac{A\epsilon_F}{N\sigma_{eff}\Gamma_{rad}(1 - e^{-\lambda t_a})e^{-\lambda t_w}\left(\frac{1 - e^{-\lambda t_c}}{\lambda t_c}\right)} \quad (4)$$

The average neutron flux was determined based on the activities of  $^{58}\text{Co}$  formed by  $^{58}\text{Ni}(n, p)^{58}\text{Co}$  reaction, which is moderated from 2.45 MeV neutrons.

Results of neutron yield, i.e., the total number of neutrons

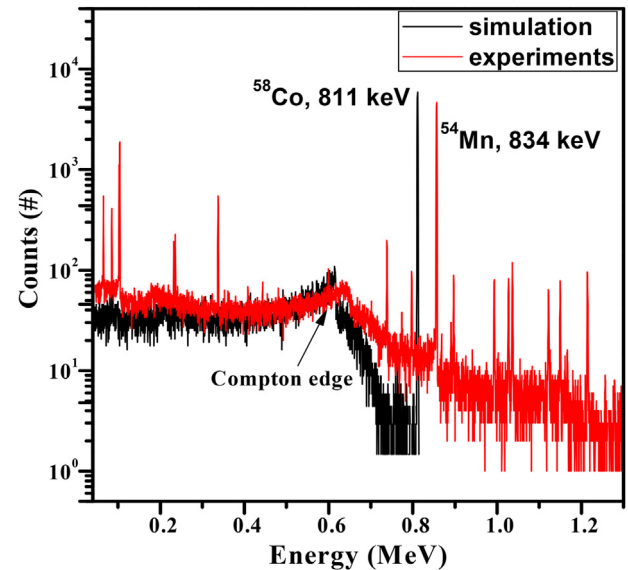


Fig. 3. The efficiency calibration of HPGe detector by the experimental method and the Monte Carlo method.

generated by fusion reaction, detected via activation of the deployed specimens at the various spots especially of the outer vessel of KSTAR are plotted in Fig. 4. Even though there is some fluctuation, the average neutron yield at each port (J, F, P and M port) shows the order of  $10^{12}$  n/s, specifically in the range from  $3.76 \times 10^{12}$  n/s to  $7.56 \times 10^{12}$  n/s. The activation analysis was repeated twice and the second experiment could reduce the data spread significantly. Activation analysis results carried out by NFRI (National Fusion Research Institute) at the inner vessel are plotted together in Fig. 4, showing that average total neutron yield was in the order of  $\sim 10^{14}$  n/s, specifically  $3 \times 10^{14}$  n/s  $\sim 5 \times 10^{14}$  n/s which are two orders of magnitude higher than those at the outer vessel. For example, the neutron yield measured by the Ni specimen installed at back-side of graphite tile of KSTAR (J port) was

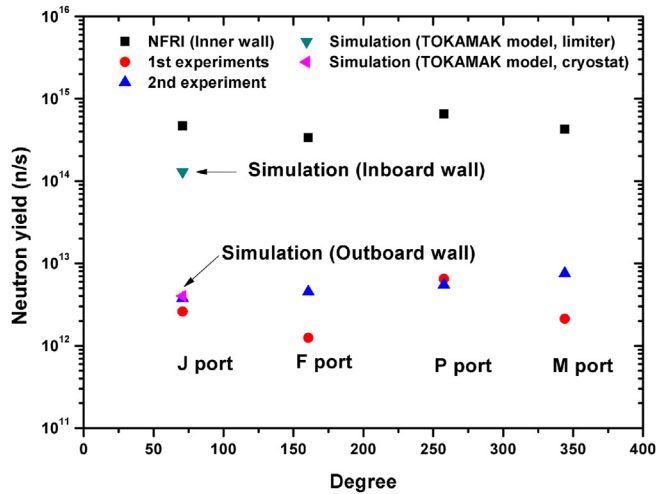


Fig. 4. Average neutron yield fluctuation with a degree at inner vessel and outer cryostat.

estimated to be  $4.65 \times 10^{14}$  n/s, as shown in Fig. 4. This yield at the inner vessel region can be estimated as the neutron generation yield of fusion reaction in the D-D plasma inside KSTAR. Remarkably, neutron yield results may show a little variation in activation analysis because plasma heating to ignite and maintain fusion reaction is not always identical at each shot, nevertheless, they showed the reproducibility in each experiment.

### 3.2. 3-Dimensional simulation based on the activation analysis

Monte Carlo simulation was carried out to confirm the neutron activation analysis results and to simulate them over whole KSTAR system using MCNP code with 3D modeling technique. Basically, Whole system modeling can handle more information on the structure and its components in detail than 40-degree model. Whole system modeling can calculate more precisely than 40-degree model, because particle interference can be occurred at the boundary of 40-degree model. Thus, in this study, whole system modeling was taken to simulate the components with the dimensional information. Simulated 3D view of the MCNP geometry in Fig. 5 (c) shows the inside structure of KSTAR such as limiter, bridge, vacuum vessel, TF (Toroidal Field) coil, and cryostat. For reference, the limiter consists of bolted graphite and 316L stainless steel. The cryostat and vacuum vessel are made of 316L stainless steel.

MCNP codes closely simulate the experiment set-up to estimate not only neutron yield but also its energy moderation while passing through each component. As demonstrated in Fig. 4, the simulation result of neutron yield was in very good agreement with the activation analysis data at J port, especially the data in the second experiment. Fig. 6 shows the simulation results of the energy spectrum of the neutrons moderated during the interaction with the KSTAR component materials.

Finally, according to the MCNP simulation, the neutron production yield at the limiter, port, and cryostat are  $5.36 \times 10^{-6}$  n,  $1.16 \times 10^{-6}$  n,  $1.65 \times 10^{-7}$  n, respectively. The outboard wall was estimated to have approximately 1/32 of the neutron yield at the inboard wall. In fact, the neutron yield in the tokamak fusion reactor is volumetric source as a ring shape, occupying the central plasma part of the vacuum chamber. 2D cross-sectional distribution of the neutron yield on XY and ZX planes of KSTAR simulated in this study are shown in Fig. 7. The neutron yield has its maximum concentration near the center of blanket and decreases with increasing proximity to the vacuum vessel wall.

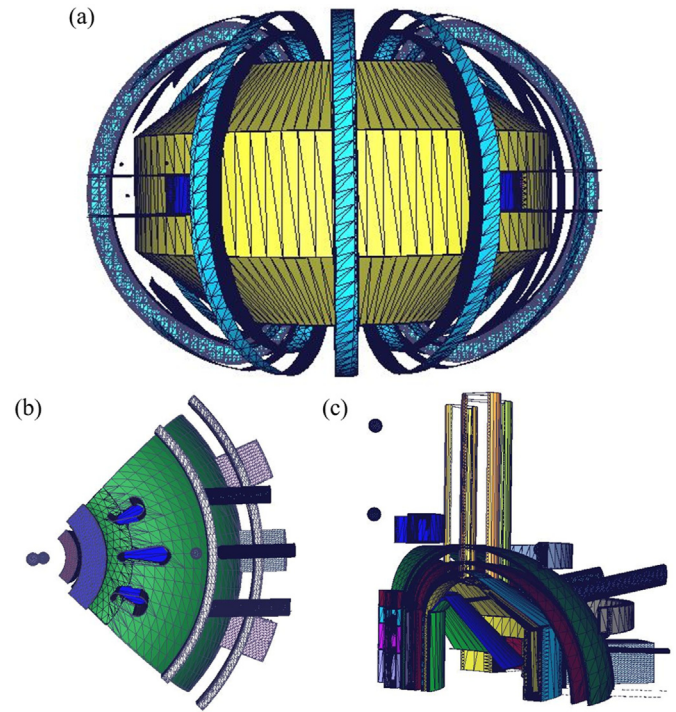


Fig. 5. The modeling for calculation of average neutron yield (a) whole body modeling of KSTAR (b) Outside structure of KSTAR (c) Inside structure of KSTAR.

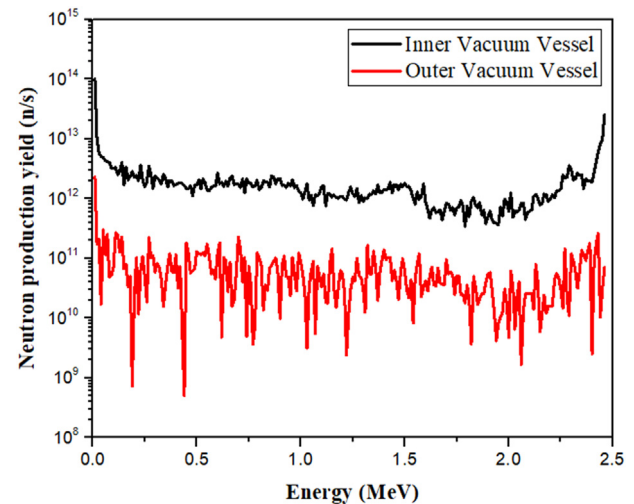
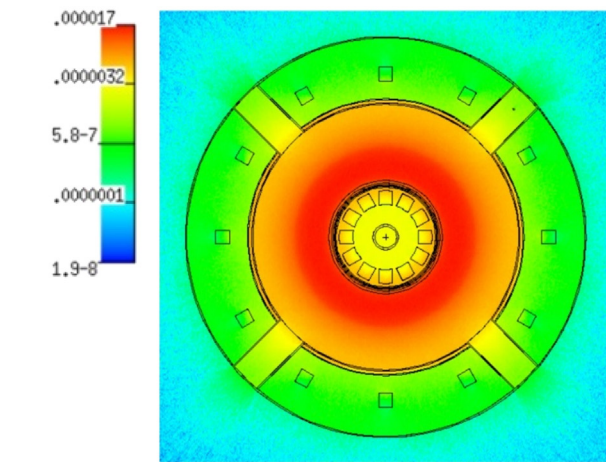


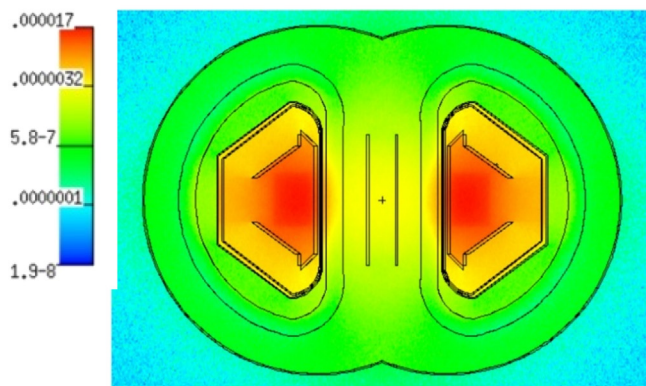
Fig. 6. MCNP calculated tendency of neutron spectra after passing through the structure.

According to simulation results, the neutron yield at the central region can be estimated as  $2.41 \times 10^{14}$  n/s by using maximum of neutron yield ( $7.56 \times 10^{12}$  n/s) measured from activation specimens. Activation analysis results carried out by the Ni specimen installed at back-side of graphite tile from NFRI researcher group at the inner vessel are plotted together in Fig. 4, showing that average total neutron yield were in the order of  $\sim 10^{14}$  n/s, specifically  $3 \times 10^{14}$  n/s  $\sim 5 \times 10^{14}$  n/s which are two order of magnitude higher than those at the outboard wall. Based on the analysis NFRI reported that they achieved first-step operation goals during KSTAR campaign in 2015. Both estimation results and activation analysis results show the good agreement with the operation goal in KSTAR.





(a) XY plane



(b) ZX plane

Fig. 7. Neutron distribution of KSTAR (a) XY plane (b) ZX plane.

#### 4. Conclusions

KSTAR is a magnetic D-D fusion device which was constructed and has been operating in Korea since June 2008. To analyze the various phenomenon related the fusion neutron such as radiation damage and material activation of the structure, the neutron yield distribution with neutron energy spectrum at the inside and outside of the vessel is necessary.

In this study, therefore, the neutron flux distribution depending on its locations was investigated with the neutron activation analysis designed to obtain the necessary information in the KSTAR system. High purity Ni specimen target foil (containing 69.08%  $^{58}\text{Ni}$ ) was selected deployed especially at the outboard wall of the KSTAR. Then, the Monte Carlo code simulation was carried out to verify the analysis results and to extend the results to 3D mapping of the neutron yield distribution in the KSTAR system. For the Monte Carlo simulation fully extended 40-degree 3D model was used to express the components with the detailed dimensional information. MCNP code was used for the simulation.

While the activation specimens were loaded, KSTAR operated for 10 days with an average of 10 shots in a day, during a total of 20 min. Total neutron yields resulting from the activation analysis

turned out to be  $3.76 \times 10^{12} \text{ n/s} - 7.56 \times 10^{12} \text{ n/s}$  at the outer wall of the KSTAR, two orders of magnitude lower than those at the inner vessel of the KSTAR. These results were verified by Monte Carlo simulation results, which demonstrate the attenuation of neutron yield while passing through the different structural materials of the reactor. These are in good agreement with previous works.

Based on the fully expanded 3-dimensional simulation results, 2D cross-sectional distributions of the neutron yield on XY and ZX planes of KSTAR were examined, revealing that the neutron yield has its maximum concentration near the center of blanket and decreases with increasing proximity to the vacuum vessel wall.

#### Declaration of competing interest

The authors declare that they have no known competing financial interests or personal relationships that could have appeared to influence the work reported in this paper.

#### Acknowledgement

This work was supported by a National Research Foundation of Korea (NRF) grant funded by the Korean government (MSIP: Ministry of Science, ICT, and Future Planning) (No. NRF-2017M2B2B1072888) and by the "Human Resources Program in Energy Technology" of the Korea Institute of Energy Technology Evaluation and Planning (KETEP), granted financial resources from the Ministry of Trade, Industry, & Energy, Republic of Korea (No. 20204030200100). And the first two author(San Chae and Jae-Yong Lee) contributed equally to this work.

#### References

- [1] A.C. England, S.G. Lee, Y.S. Lee, Z.Y. Chen, J.W. Yoo, W.C. Kim, J.G. Kwak, M. Kwon, Neutron emission from KSTAR Ohmically heated plasmas, *Phys. Lett., A* 375 (2011) 3095–3099.
- [2] J.-G. Kwak, Y.S. Lee, D.R. Lee, C.S. Kim, H.S. Kim, H.J. Lee, K. Shinohara, Accumulated 2-D neutron flux distribution during KSTAR operation, *Fusion Eng. Des.* 136 (2018) 777–781.
- [3] R.R. Greenberg, P. Bode, E.A. De Nadai Fernandes, Neutron activation analysis: a primary method of measurement, *Spectrochim. Acta B Atom Spectrosc.* 66 (2011) 193–241.
- [4] C.C. Negoita, Measurement of Neutron Flux Spectra in a Tungsten Benchmark by Neutron Foil Activation Method, Shaker, Germany, 2004.
- [5] K. Ehrlich, Materials research towards a fusion reactor, *Fusion Eng. Des.* 56–57 (2001) 71–82.
- [6] A.F. Rowcliffe, L.M. Garrison, Y. Yamamoto, L. Tan, Y. Katoh, Materials challenges for the fusion nuclear science facility, *Fusion Eng. Des.* 135 (2018) 290–301.
- [7] A.F. Rowcliffe, C.E. Kessel, Y. Katoh, L.M. Garrison, L. Tan, Y. Yamamoto, F.W. Wiffen, Materials-engineering challenges for the fusion core and lifetime components of the fusion nuclear science facility, *Nucl. Mater. Energy* 16 (2018) 82–87.
- [8] A.V. Spitsyn, N.P. Bobyr, T.V. Kulevoy, P.A. Fedin, A.I. Semennikov, V.S. Stolbunov, Use of MeV energy ion accelerators to simulate the neutron damage in fusion reactor materials, *Fusion Eng. Des.* 146 (2019) 1313–1316.
- [9] O.N. Jarvis, E.W. Clipsham, M.A. Hone, B.J. Laundry, M. Pillon, M. Rapisarda, G.J. Sadler, P. van Belle, K.A. Verschuur, Use of activation technique for the measurement of neutron yields from deuterium plasmas at the joint European torus, *Fusion Technol.* 20 (1991) 265–284.
- [10] S. Jednorog, E. Laszynska, P. Batistoni, B. Bienkowska, A. Cufar, Z. Ghani, L. Giacomelli, A. Klix, S. Loreti, K. Mikszuta, L. Packer, A. Peacock, M. Pillon, S. Popovichev, M. Rebai, D. Rigamonti, N. Roberts, M. Tardocchi, D. Thomas, Activation measurements in support of the 14MeV neutron calibration of JET neutron monitors, *Fusion Eng. Des.* 125 (2017) 50–56.
- [11] R.C. Koch, Chapter 3 - activation analysis • experimental methods, in: R.C. Koch (Ed.), *Activation Analysis Handbook*, Academic Press, 1960, pp. 11–15.
- [12] R.C. Koch, Chapter 2 - activation analysis • theoretical considerations, in: R.C. Koch (Ed.), *Activation Analysis Handbook*, Academic Press, 1960, pp. 5–10.
- [13] C.S. Kim, S.P. Hong, M.S. Cheon, B.S. Kang, S. Cho, Neutron diagnostics using Compton suppression gamma-ray spectrometer for tritium breeding blanket experiments, *Fusion Eng. Des.* 109–111 (2016) 88–92.
- [14] K. Tian, P. Calderoni, B.-E. Ghidersa, A. Klix, Feasibility study of a neutron activation system for EU test blanket systems, *Fusion Eng. Des.* 109–111

- (2016) 1517–1521.
- [15] MCNP — a General Monte Carlo N-Particle Transport Code, Version 5, 2000.
- [16] T. Vasilopoulou, I.E. Stamatelatos, P. Batistoni, N. Fonnesu, R. Villari, J. Naish, S. Popovichev, B. Obryk, Activation foil measurements at JET in preparation for D-T plasma operation, *Fusion Eng. Des.* 146 (2019) 250–255.
- [17] F.H. Stefaan pomme, Piotr Robouch, Nestor Etxebarria, Gorka Arana, Neutron activation analysis with K0-standardisation: general formalism and procedure, in: SCK-CEN, SCK-CEN, 1997.
- [18] M.B. Chadwick, M. Herman, P. Obložinský, M.E. Dunn, Y. Danon, A.C. Kahler, D.L. Smith, B. Pritychenko, G. Arbanas, R. Arcilla, R. Brewer, D.A. Brown, R. Capote, A.D. Carlson, Y.S. Cho, H. Derrien, K. Guber, G.M. Hale, S. Hoblit, S. Holloway, T.D. Johnson, T. Kawano, B.C. Kiedrowski, H. Kim, S. Kunieda, N.M. Larson, L. Leal, J.P. Lestone, R.C. Little, E.A. McCutchan, R.E. MacFarlane, M. MacInnes, C.M. Mattoon, R.D. McKnight, S.F. Mughabghab, G.P.A. Nobre, G. Palmiotti, A. Palumbo, M.T. Pigni, V.G. Pronyaev, R.O. Sayer, A.A. Sonzogni, N.C. Summers, P. Talou, I.J. Thompson, A. Trkov, R.L. Vogt, S.C. van der Marck, A. Wallner, M.C. White, D. Wiarda, P.G. Young, ENDF/B-VII.1 nuclear data for science and technology: cross sections, covariances, fission product yields and decay data, *Nucl. Data Sheets* 112 (2011) 2887–2996.